Supplement of Atmos. Chem. Phys., 17, 14501–14517, 2017
https://doi.org/10.5194/acp-17-14501-2017-supplement


Atmospheric Chemistry and Physics
Open Access
EGU

*Supplement of*

# Field characterization of the $PM_{2.5}$ Aerosol Chemical Speciation Monitor: insights into the composition, sources, and processes of fine particles in eastern China

**Y. Zhang et al.**

*Correspondence to:* Lili Tang (lily3258@163.com) and Yele Sun (sunyele@mail.iap.ac.cn)

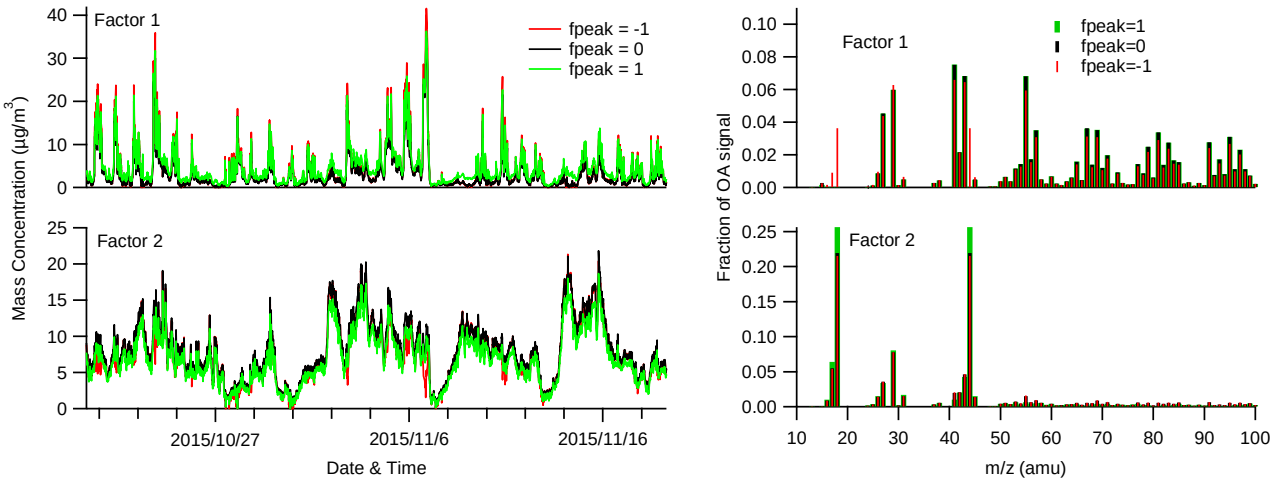


**Figure S1.** Time series and mass spectral profiles for the 2-factor PMF solution of the $PM_1$ ACSM dataset at three different fpeak values.

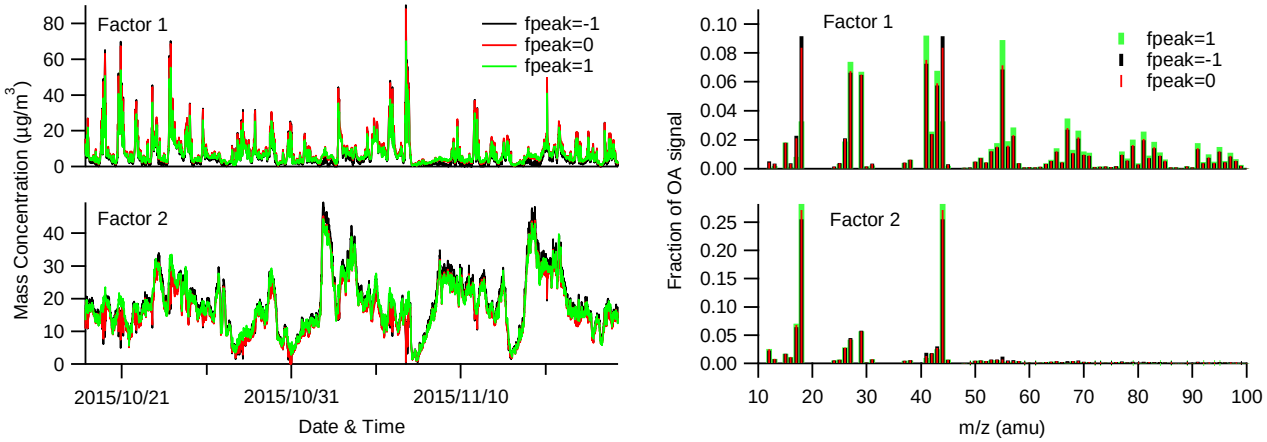


**Figure S2.** Time series and mass spectral profiles for the 2-factor PMF solution of the $PM_{2.5}$ ACSM dataset at three different fpeak values.

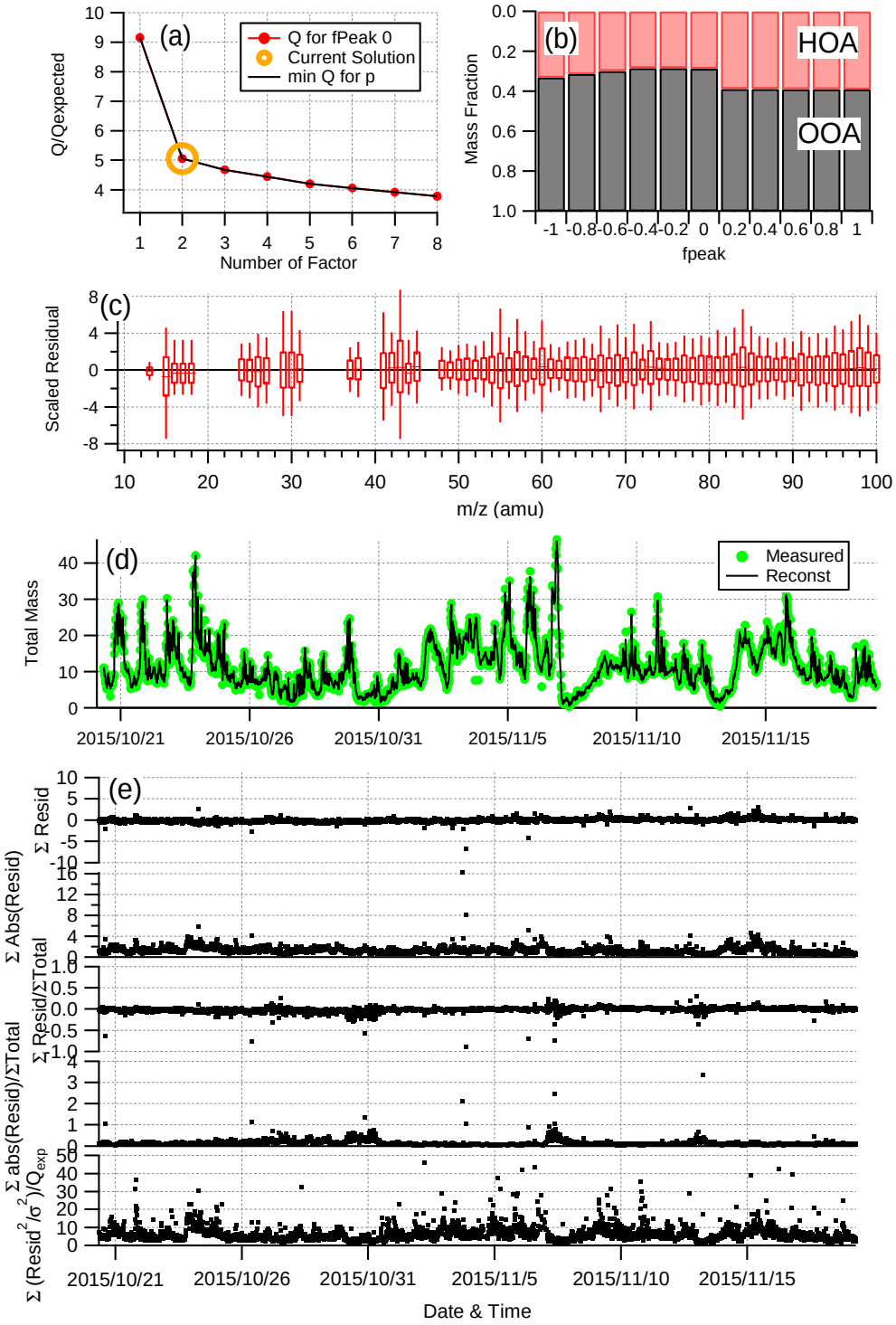


**Figure S3.** Summary of key diagnostic plots of the $PM_1$-ACSM PMF results for the 2-factor solution: (a) $Q/Q_{exp}$ as a function of the number of factors, (b) mass fraction of OOA and HOA as a function of FPEAK, (c) box and whiskers plot showing the distributions of the scaled residuals for each m/z, (d) comparison of the measured mass with the PMF reconstructed mass, (e) time series of the residual diagnostics and $Q/Q_{exp}$ for each point in time.

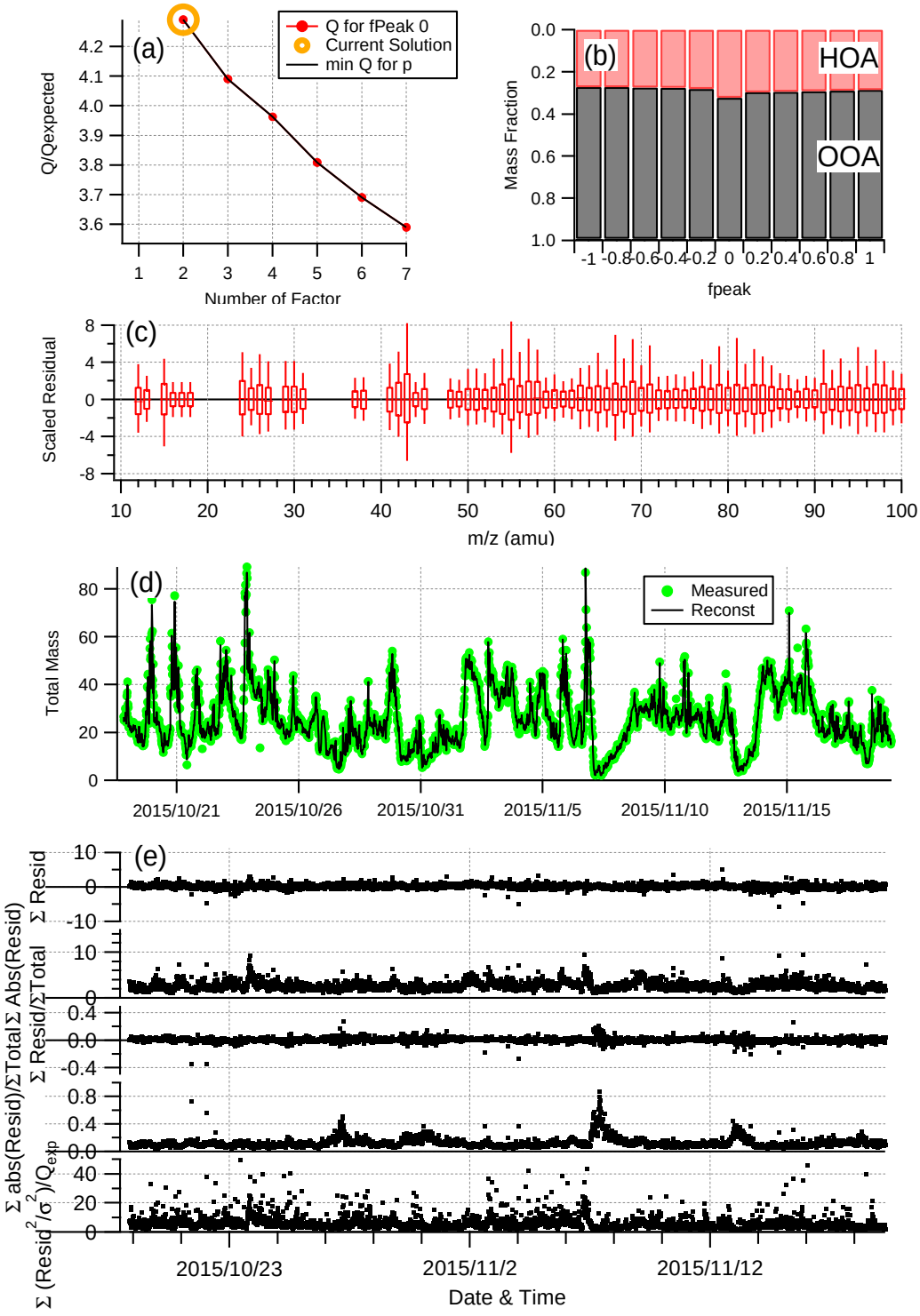


**Figure S4.** Summary of key diagnostic plots of the $PM_{2.5}$-ACSM PMF results for the 2-factor solution: (a) $Q/Q_{exp}$ as a function of the number of factors, (b) mass fraction of OOA and HOA as a function of FPEAK, (c) box and whiskers plot showing the distributions of the scaled residuals for each m/z, (d) comparison of the measured mass with the PMF reconstructed mass, (e) time series of the residual diagnostics and $Q/Q_{exp}$ for each point in time.

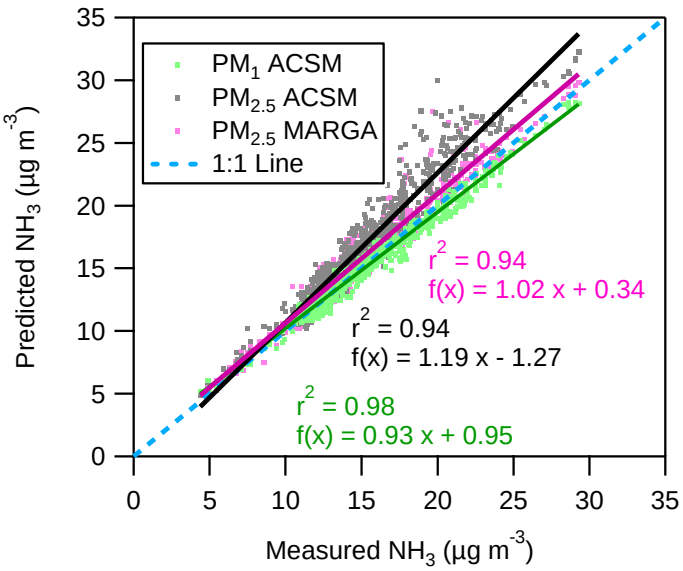


**Figure S5.** Comparison of measured $NH_3$ and predicted $NH_3$ with inputs of $PM_1$-ACSM (without MARGA's $Na^+$, $Ca^{2+}$, $K^+$, $Mg^{2+}$), $PM_{2.5}$-ACSM (with MARGA's $Na^+$, $Ca^{2+}$, $K^+$, $Mg^{2+}$), and $PM_{2.5}$-MARGA (with $Na^+$, $Ca^{2+}$, $K^+$, $Mg^{2+}$) data, respectively, and same gas-phase $HNO_3$ and $NH_3$, ambient RH, T for all predictions.

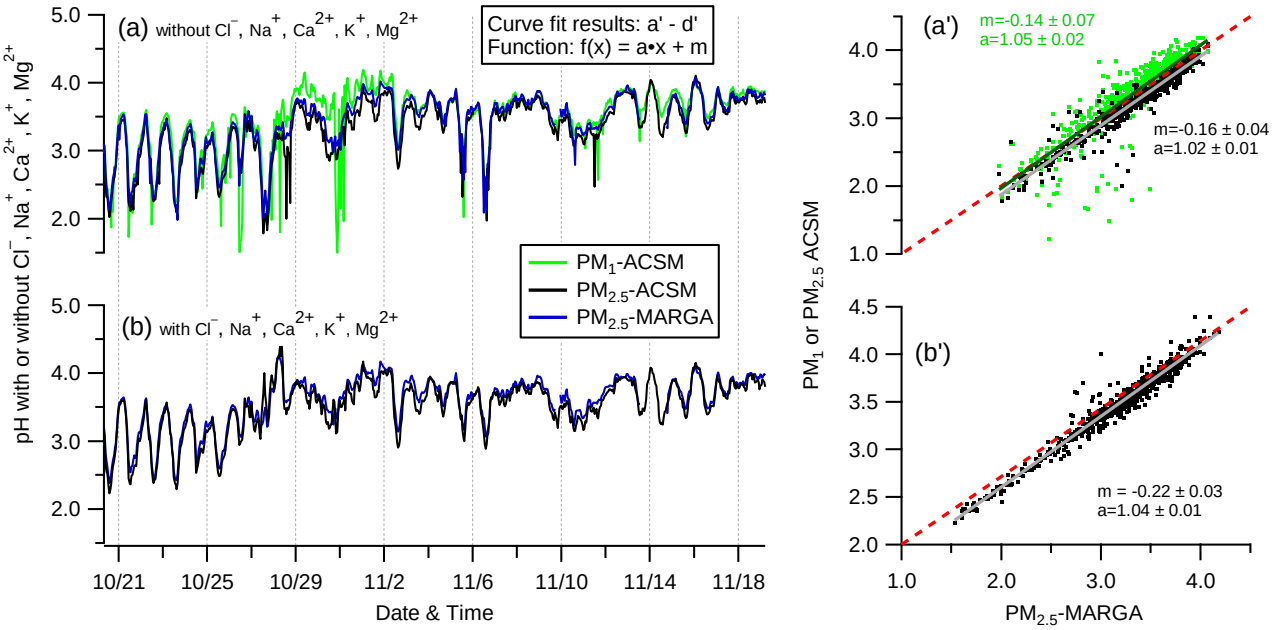


**Figure S6.** Comparisons of ISORROPIA-II-predicted aerosol pH for the data from different instruments (i.e., $PM_1$-ACSM, $PM_{2.5}$-ACSM, and $PM_{2.5}$-MARGA), respectively. The $SO_4^{2-}$ – $NO_3^-$ – $NH_4^+$ – $Cl^-$ – $Na^+$ – $Ca^{2+}$ – $K^+$ – $Mg^{2+}$ – $HNO_3$ – $NH_3$ – $H_2O$ system and the $SO_4^{2-}$ – $NO_3^-$ – $NH_4^+$ – $HNO_3$ – $NH_3$ – $H_2O$ system were used for the prediction, respectively.

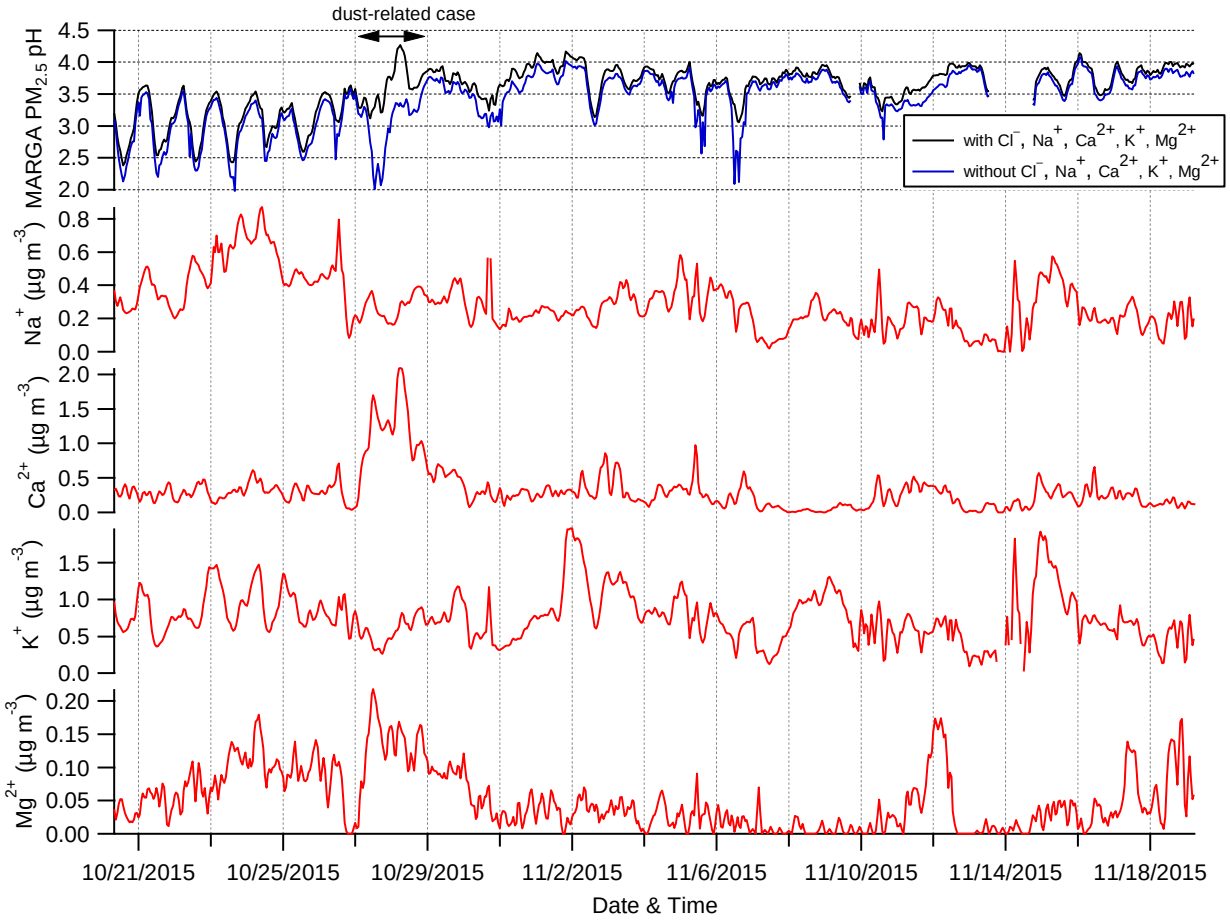


**Figure S7.** Time series of fine particle pH predicted with the MARGA data sets for different model systems, i.e., with and without $Na^+$, $Ca^{2+}$, $K^+$, $Mg^{2+}$, and the mass concentrations of $Na^+$, $Ca^{2+}$, $K^+$, and $Mg^{2+}$.

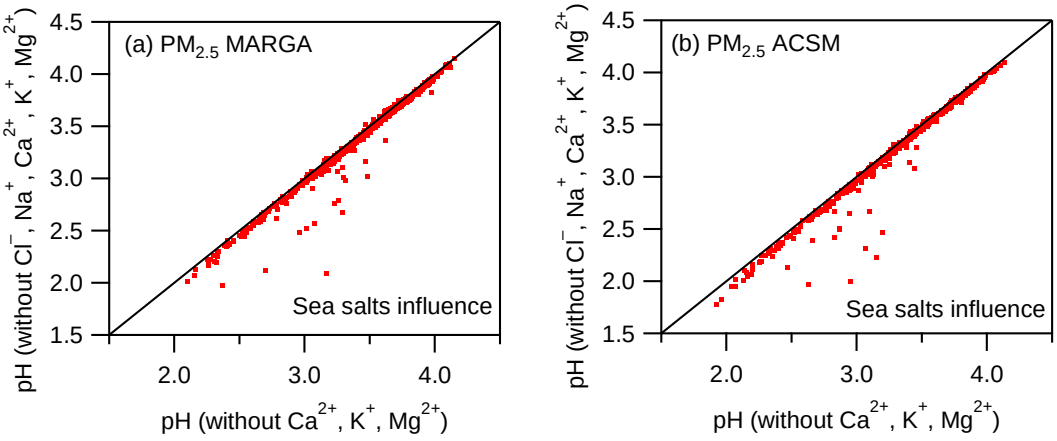


**Figure S8.** Comparisons of ISORROPIA-II-predicted fine aerosol pH with and without sea salts influence for the $PM_{2.5}$ MARGA (a) and Q-ACSM (b), respectively.

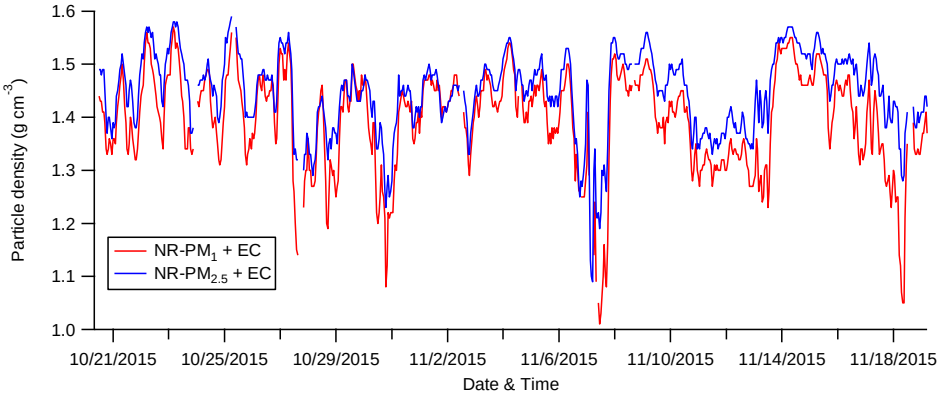


**Figure S9.** Time series of chemical-dependent dry density of $PM_1$ and $PM_{2.5}$ particles. The calculated density (g $cm^{-3}$) varies from 1.01 (1.09) to 1.57 (1.75) with the mean value being 1.39 (1.44) for $PM_1$-Q-ACSM ($PM_{2.5}$-Q-ACSM).

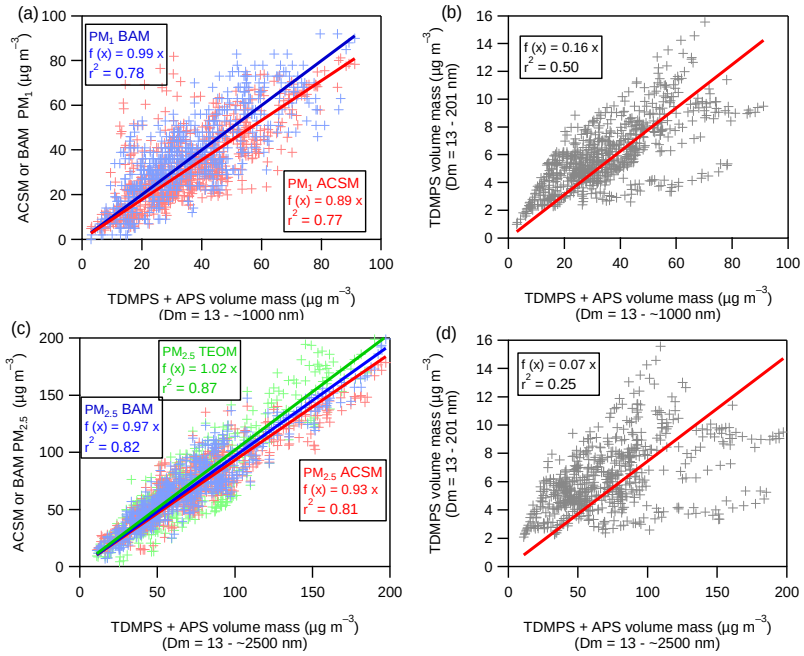


**Figure S10.** Correlations between the $PM_1$-ACSM, $PM_{2.5}$-ACSM, $PM_1$-BAM, $PM_{2.5}$-BAM and the volume-dependent mass (TDMPS and APS) with the particle density being calculated from the chemical species of the $PM_1$-ACSM and $PM_{2.5}$-ACSM, respectively. On average, the $PM_1$ and $PM_{2.5}$ Q-ACSM total dry mass accounts for respectively 89 % and 93 % of the $PM_1$ and $PM_{2.5}$ volume-dependent mass concentrations. As reported by Xu et al. (2017a), the $PM_{2.5}$ lens system showed a significant particle loss at below around 200 nm, with a lower transmission efficiency of 45 % on average. Considering this, we estimated that the lost of small particles at size ~13 – 201 nm might account for around 3 % of the total volume-dependent $PM_{2.5}$ mass (Fig. S10d).

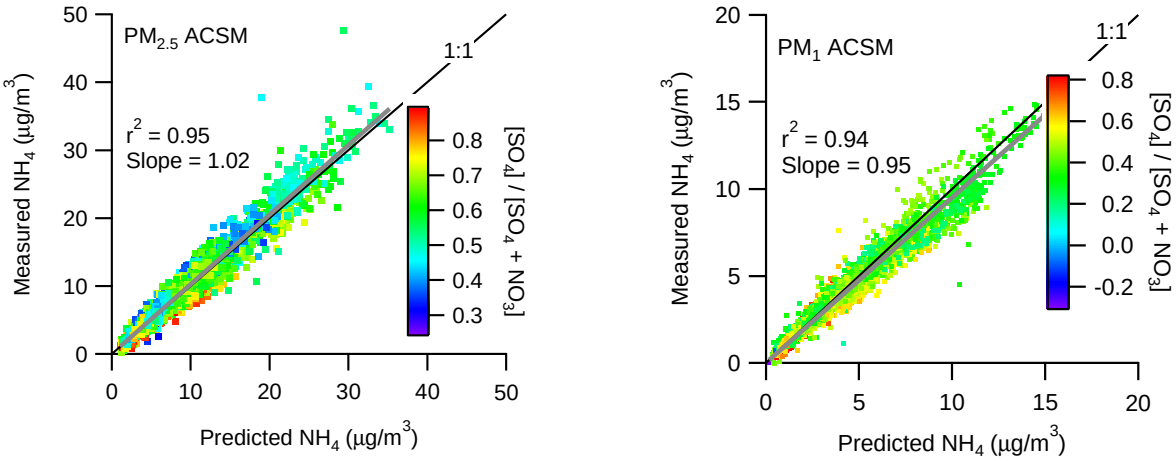


**Figure S11.** Relationship between the measured $NH_4$ and predicted $NH_4$ for both the $PM_{2.5}$ and $PM_1$ ACSMs, respectively. The points in the plots are colored by the ratio of $[SO_4]$ / $[SO_4/NO_3]$. Note that the predicted $NH_4$ is estimated by $18 \times (2\times[SO_4/96] + [NO_3/62] + [Cl/35.5])$.

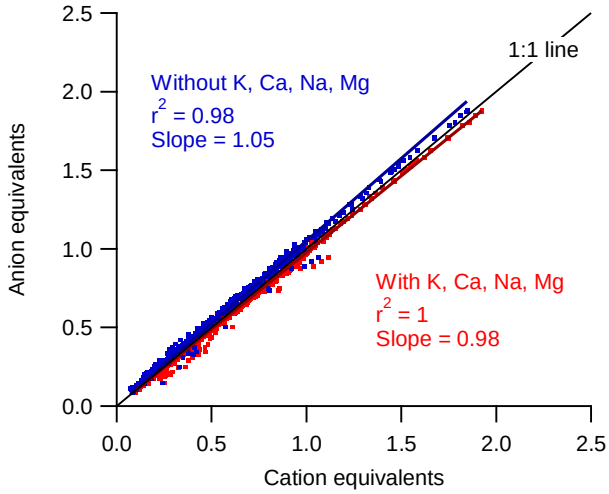


**Figure S12.** Ion balance of the water-soluble ions measured by the $PM_{2.5}$ MARGA. Note that: anion equivalents = $[NH_4^+/18] + [Na^+/23] + [K^+/39] + [Mg^{2+}/12] + [Ca^{2+}/20]$, and cation equivalents = $[SO_4^{2-}/48] + [NO_3^-/62] + [Cl^-/35.5]$, in which the chemical ions are in the unit of µg $m^{-3}$.

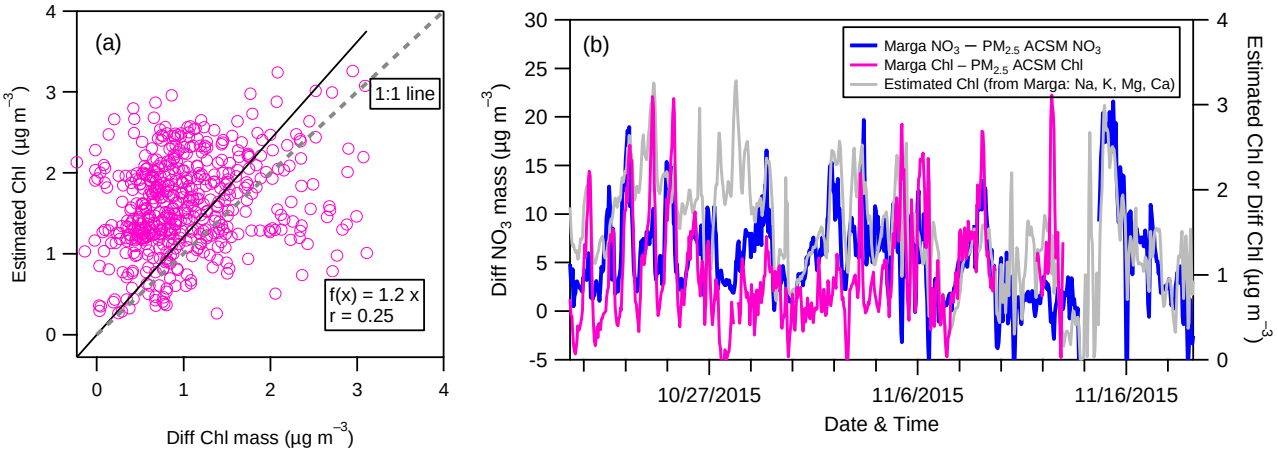


**Figure S13.** Relationship between the measured nitrate and chloride difference values (i.e., $PM_{2.5}$-Marga – $PM_{2.5}$-ACSM) and the estimated maximum chloride by mass balance from $Na^+$, $Ca^{2+}$, $K^+$, and $Mg^{2+}$.

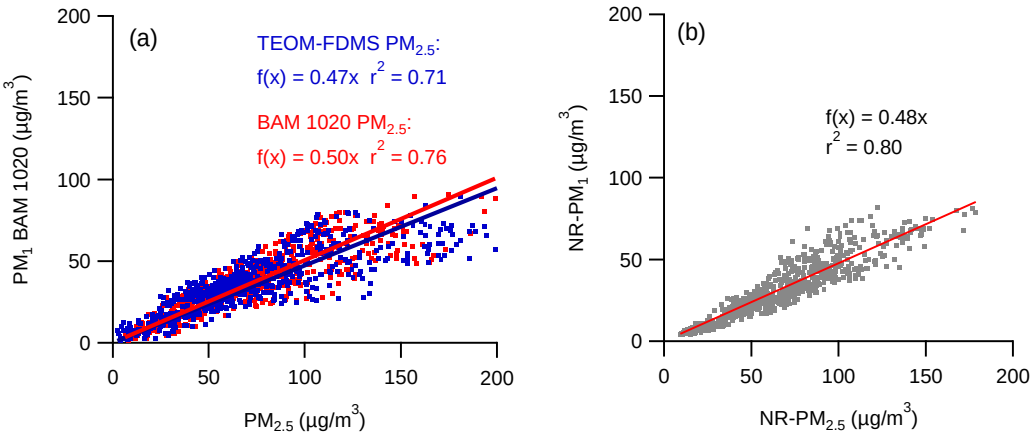


**Figure S14.** Relationships between (a) the $PM_1$ (measured by Met one BAM1020) and total $PM_{2.5}$ (measured by TEOM-FDMS and Met one BAM1020 respectively) mass loadings; and (b) the non-refractory NR-$PM_1$ (measured by the $PM_1$ ACSM) and $PM_{2.5}$ (NR-$PM_{2.5}$ measured by the $PM_{2.5}$-ACSM) for the entire study.

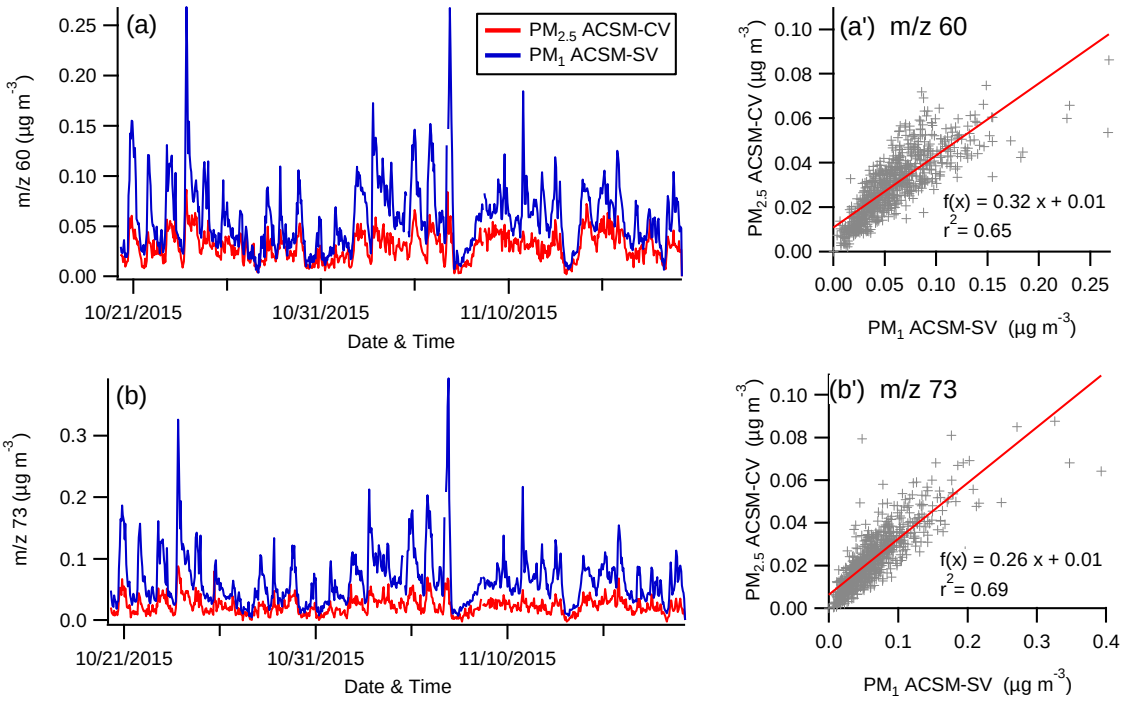


**Figure S15.** Time series (a-b) and correlation (a'-b') of the mass concentration *m/z* 60 and *m/z* 73 from the $PM_{2.5}$-ACSM and $PM_1$-ACSM, respectively.

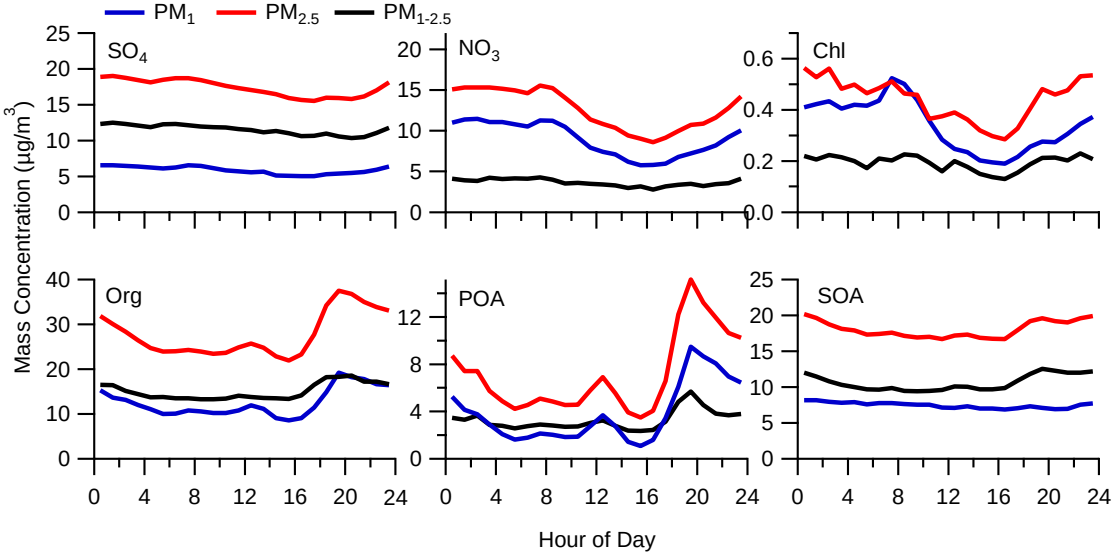


**Figure S16.** Sized-segregated diurnal variations of the fine aerosol species and organic components.

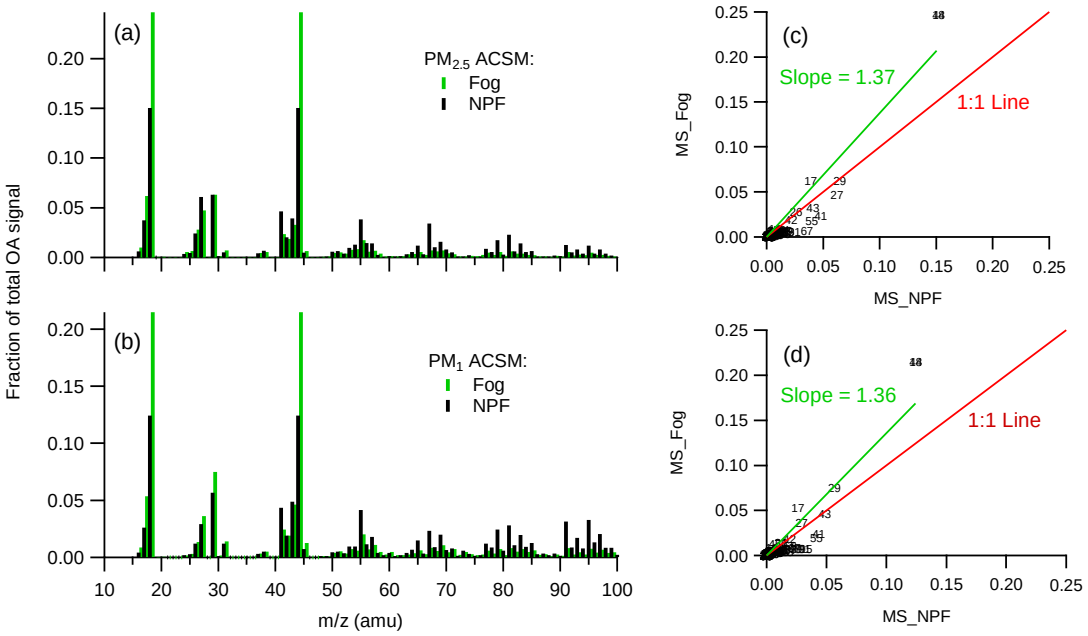


**Figure S17.** Averaged mass spectra (MS) of OA for the $PM_1$ and $PM_{2.5}$ ACSM during the new particle formation (NPF, Episode 2) and the fog event (Fog, Episode 5) periods, respectively.

**Table S1.** Thermal protocol used in this study within the Sunset Lab. Semi-Continuous OC/EC Analyzer

| Gas | Hold time (s) | Temperature (˚C) |
|---|---|---|
| He | 10 | 1 |
| He | 95 | 600 |
| He | 95 | 840 |
| He | 30 | Oven off |
| He | 5 | 550 |
| $He/O_2$ | 10 | 550 |
| $He/O_2$ | 25 | 550 |
| $He/O_2$ | 45 | 650 |
| $He/O_2$ | 115 | 870 |